Wave power calculation of a large periodic array of bottom-hinged paddle wave energy converters using Floquet-Bloch theory

Jin Huang[a], Richard Porter[a]

[a]School of Mathematics, University of Bristol, Fry Building, Woodland Road, Bristol, BS8 1UG, UK

Abstract

In this study we consider a wave energy farm consisting of a large number of bottom-hinged paddles. The paddles are arranged in a doubly-periodic manner, with a finite number of identical rows and each row containing an infinite number of paddles. Each paddle is attached to its own damper and spring, allowing power to be generated through its pitching motion. Unlike previous studies into paddle arrays, we envisage compact arrays consisting of small devices arranged across a large number of rows. The mathematical analysis of this proposed configuration is best suited to methods that exploit the periodicity of the array. It is shown that the velocity potential everywhere within the array can be described by an expansion in terms of suitably-defined Floquet-Bloch eigenmodes and this allows the solution to the scattering problem involving waves incident upon the array to be determined by a simple low-order system of equations. The method used in this study is exact within the setting of linearised water waves and has all of the advantages of classical low-frequency multi-scale homogenization without the low-frequency restriction. It may also be regarded as a natural extension of the well-known wide-spacing approximation without the large separation restriction. Although the focus of this paper is on the mathematical approach to the solution of the problem, we provide a range of results to illustrate the performance of this proposed wave energy converter concept.

Keywords: Floquet-Bloch theory, Periodic array, Wave energy

1. Introduction

One of the earliest concepts for a wave energy harvesting device consisted of a paddle partially immersed through the water surface [1], which could extract power from propagating waves through the damping of its pitching motion about a hinge located above the surface. This initial idea rapidly evolved into a more sophisticated design, which became known as Salter's Duck [2]: a long device, cam-shaped in cross-section, able to pitch about a central axis. The flat front of the cam acts as a paddle to absorb plane incident waves and its rounded behind suppresses downwave radiation. Subsequently, a variety of competing design concepts for wave energy devices have been developed whose operation is often underpinned by theoretical principles (for a detailed description see [3]). For example, a symmetric paddle operating in pitch motion symmetrically about a vertical plane was theoretically shown to have a maximum efficiency in converting incident wave power of 50% whereas the asymmetry of Salter's Duck allowed it to become, in principle, 100% efficient at certain frequencies [4]. It was some time later, in the mid-2000s, that the original hinged paddle concept returned, being developed into "Oyster" [5] a single device tested at full scale and capable of generating 800kW peak power. Despite the shortcomings of a paddle-like design in a two-dimensional setting, it has been demonstrated theoretically, computationally and experimentally that a long paddle could take advantage of three-dimensional end effects allowing it to possess broadband energy capture characteristics [6, 7, 8]. Always conceived as being deployed in arrays, work was also performed towards array optimisation [9, 10, 11, 12, 13, 14] as well as shape optimisation [15].

A sharp drop in the cost of solar and wind renewables and a reduction in the support needed to sustain the commercial development of wave renewables sadly ended the Oyster project. One of the many challenges faced by Oyster and other wave renewables is the cost of installation, reliability of operation and maintenance. One means of mitigating this is to develop wave energy harvesting devices which are small and modular and which are employed in large compact arrays. In this paper we consider the operation of large periodic arrays of submerged hinged paddle devices in which we imagine each element being narrow in relation to the original Oyster units conceived in [5]. This makes the work distinct from previous studies on arrays for example, [13] whose work is related to just two periodic rows of flaps or [12, 14] who consider the optimal placement of a finite number of full-sized Oyster devices (approximately 25m in width and 12m in height).

Water wave interaction with regular arrays of fixed marine structures has been a subject of interest to engineers and researchers in the context of, for example, sand bars [16, 17], supporting columns of offshore structures [18, 19], coastal breakwater schemes [20], and as a water wave metamaterial for the bespoke manipulation of waves [21]. If the elements in the array move in response to the fluid motion as in [22, 23], the situation becomes more complicated, and direct methods of solution, in which multiple scattering and radiation of waves between every pair of elements in the array are exactly accounted for, become increasingly computationally expensive as the number of elements grows. It is therefore not surprising that methods have been developed to reduce the effort in making calculations for large arrays. Efficient and stable methods, such as the scattering matrix method [24], and the transfer matrix method [17], can simultaneously transfer propagating and evanescent modes information between adjacent elements of the array, thus allowing the connection between the incident, reflected and transmitted waves to be made. If the distance between the elements is large compared to the wavelength so that the evanescent modes can be assumed to have decayed sufficiently, one can further reduce the complexity to develop approximations referred to as wide-spacing and/or point absorber assumptions [25]. This approach has been recently adopted by [26] in a study similar to the one being undertaken in this paper. For arrays without the periodicity, approaches can be algorithmic such as [27] who approaches array interaction in hierarchical clusters or numerical such as [12, 14] who modelled flap-type oscillating wave surge converters by using Green's integral theorem.

Alternatively, one may be able to exploit a contrast in physical lengthscales in the problem (typically between the wavelength and the array spacing) and employ homogenisation methods as in [21, 22, 23] to replace the effect of fixed/moving structures by simpler effective medium equations/boundary conditions. For example, [19, 22, 28] considered wave attenuation due to viscous damping of the fluid motion triggered by eddy-induced vorticity, through flexible marine vegetation, and modelled using linearised Reynolds Average Navier Stokes equations. Also, [23] investigated wave energy absorption by large compact arrays of buoys floating on the water surface generating power through their heave motion, using homogenisation to derive an effective free surface condition.

In this study we will consider a periodic array consisting of vertical paddles bottom-hinged on the sea bed. It should be noted that for our array of narrow paddles operating in regular waves close to the coastline, the length scales are different from the work mentioned above. The paddles are envisaged to be 1-2 m in width rather than 10-20 m across and with a close spacing (roughly 2 m apart) in contrast to the assumptions adopted by [26]. Whilst there will be turbulent energy shed into the fluid especially from the edges of the paddles, we assume that the damping mechanism due to the mechanical power take-off acting on the paddles will be dominant. With the purpose of simplifying the problem, we are therefore going to assume in this work that the fluid is inviscid and its motion irrotational and energy is only lost to the power take-off mechanism attached to the paddles, without including viscous effects considered in [19, 22].

In Section 2, we consider plane waves obliquely incident upon an array of paddles which extend indefinitely and periodically in the longshore direction and consist of a finite number, M, of parallel rows that extend periodically in the perpendicular direction. The fluid is assumed to extend to infinity in all directions with a constant depth which is assumed to be sufficiently shallow for the paddles to be connected, via hinges, to the bed. Thus various practical considerations affecting a real wave farm including finite-size effects, variable bathymetry and shoreline effects are overlooked.

The method developed in this study is based on the recent work of [29, 30] who showed that the solution throughout the domain occupied by the paddle array can be expressed exactly, and without approximation, in terms of the eigenvalues and eigenmodes of a suitably specified Floquet-Bloch problem corresponding to the corresponding infinite periodic array (this is considered in Section 3). In allowing the paddles to pitch in response to the fluid motion under the resistance of springs and dampers, we encounter some additional complexity when compared to the problem considered by [30] in which the paddles are fixed. In particular, the addition of damping implies that the eigenvalues of the Floquet-Bloch problem are no longer located along certain lines in the complex plane and locating eigenvalues in the complex plane is the main computational difference and challenge.

The mathematical approach used here has all of the advantages of classical low-frequency multi-scale homogenization in that the solution everywhere within the periodic array is determined by a fundamental "micro-scale" cell

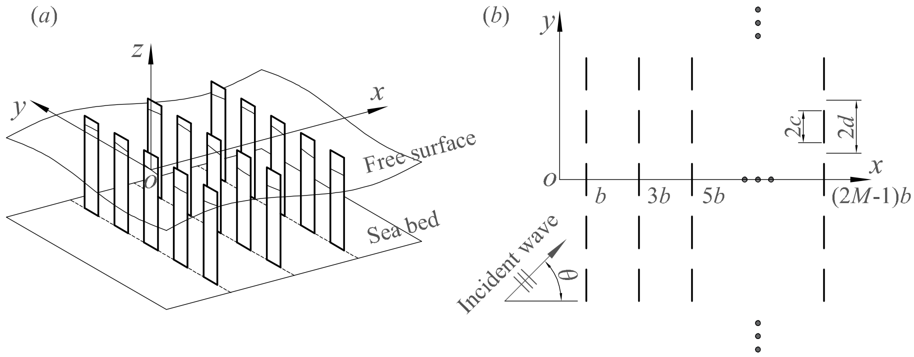

Figure 1: A periodic array of submerged hinged paddles: (a) bird's-eye view; (b) plane view.

problem (e.g. [23, 30]), but without being restricted to low frequencies. It also encodes all of the array propagation information included in transfer matrix methods referred to earlier without the associated linear algebra. Otherwise, the formulation and solution to the fundamental cell problem including a single paddle as specified by Floquet-Bloch theory are quite different from the approaches described in, for example, [8, 10, 12, 13, 17, 20, 24]. First, by combining the kinematic and dynamic boundary conditions that apply to the paddle we are not required to develop and combine solutions for separate diffraction and radiation problems which is the traditional approach (e.g. [25]) to determining the hydrodynamic response of oscillating bodies. Secondly, we avoid the complications associated with having to solve hypersingular integral equations that result from the use of Green's functions by instead using simple separation solutions in the rectangular domain of the fundamental cell of the Floquet-Bloch problem and solving the resulting integral equations using a standard Galerkin approximation.

The solution to the problem of a finite array under the excitation of incident waves requires the matching of the solution within the periodic array with solutions that hold in the two semi-infinite exterior domains, which is considered in Section 4. Here, certain orthogonality relations relating to the Floquet-Bloch eigensolutions, established in Appendix A facilitate this matching in a manner as natural as using standard eigenfunction expansions. This results in a simple low-order system of equations whose solutions determine the reflection, transmission and absorption of wave energy. In Section 4 we also produce results which focus on how absorption is affected by array spacing, incident wave angle, spring and damper settings and the number of arrays, M, included in the array. Finally, the work is concluded in Section 5.

2. Modelling and assumptions

Three-dimensional Cartesian coordinates (x, y, z) are chosen with z directed upwards and $z = 0$ coinciding with the rest position of the free surface of a fluid of density ρ and constant depth h. As shown in Fig. 1, we consider an array of identical buoyant paddles of width $2c$ attached to the sea bed via hinges located on the sea bed at regular spacings in both the x and y directions. The paddles extend uniformly through the depth of the fluid and are assumed to be thin from back to front, relative to their other dimensions, and thus the thickness of the paddle, t, is neglected in the following boundary conditions. We consider the case where the distribution of paddles is long in the y direction relative to its extent in the x direction, so we assume that there are M rows of paddles located at $x = (2m-1)b$ for $m = 1, 2, \cdots, M$ while they extend indefinitely in the y direction with a period $2d > 2c$ such that the gap between two adjacent paddles is $2a$. We also assume that the paddle is formed by a homogeneous material of density $\rho_p < \rho$, allowing the buoyancy to be altered. The axes of the hinges are aligned with the y direction so that the paddles can move in pitch. A mechanical spring with linear spring constant κ is used to provide an additional restoring moment to the paddle, whilst another moment is supplied at the hinge by a linear damper with the damping rate, γ. A plane wave of angular frequency ω is incident on the array from $x = -\infty$ directed an angle θ to the positive x-axis. Under the action of waves, energy can be extracted from water waves through the damper.

The fluid is incompressible and inviscid and the motion is assumed to be irrotational and of small amplitude, allowing it to be described by a velocity potential $\mathrm{Re}[\phi(x, y, z)e^{-i\omega t}]$. The time-independent velocity potential thus satisfies the Laplace equation, i.e.

$$\nabla^2\phi = 0, \quad \text{in the fluid,} \tag{1}$$

with the combined linearised kinematic and dynamic conditions on the free surface enforced by

$$\frac{\partial\phi}{\partial z} = \frac{\omega^2}{g}\phi, \quad \text{on } z = 0, \tag{2}$$

and no-flow condition on the fluid bottom described by

$$\frac{\partial\phi}{\partial z} = 0, \quad \text{on } z = -h. \tag{3}$$

On both sides of the paddle surface $S^{\pm}_{mn} = \{x = (2m-1)b^{\pm}, -c + 2nd < y < c + 2nd, -h < 0 < z\}$ for $m = 1, 2, \cdots, M$ and $N \in \mathbb{Z}$, the velocity potential $\phi(x, y, z)$ also satisfies the corresponding kinematic and dynamic conditions. We consider small-amplitude motions of the paddle about $z = -h$, described by the pitch angle σ_{mn} for each paddle. The linearised kinematic condition is thus given by

$$\frac{\partial\phi}{\partial x} = -\mathrm{i}\omega\sigma_{mn} f(z), \quad \text{on } S^{\pm}_{mn}, \tag{4}$$

where

$$f(z) = z + h. \tag{5}$$

The dynamic condition is expressed as

$$(-\omega^2 I - \mathrm{i}\omega\gamma + \kappa + C)\sigma_{mn} = F_{mn}, \quad \text{on } S^{\pm}_{mn}, \tag{6}$$

where $I = 2\rho_p cth(h^2/3 + t^2/12)$ is the inertia moment and $C = \rho gct(h^2 + t^2/6) - \rho_p gcth^2$ is the hydrostatic moment due to buoyancy. In this study, we choose $\rho_p = \rho/2$ and $t = h/10$ as representative values of a real device. The hydrodynamic moment on the corresponding paddle is

$$F_{mn} = -\mathrm{i}\omega\rho \int_{-h}^{0}\int_{-c}^{c} \Delta\phi_{mn}(y, z) f(z)\mathrm{d}y\mathrm{d}z, \tag{7}$$

where $\Delta\phi_{mn}(y, z) = \phi((2m-1)b^+, y + 2nd, z) - \phi((2m-1)b^-, y + 2nd, z)$ representing the potential jump across the paddle. Eliminating the paddle's angular displacement σ_{mn} between Eqs. (4) and (6) results in the following combined kinematic and dynamic conditions

$$\frac{\partial\phi}{\partial x} = -\frac{\tau f(z)}{dh^4}\int_{-h}^{0}\int_{-c}^{c} \Delta\phi_{mn}(y, z) f(z)\mathrm{d}y\mathrm{d}z, \quad \text{on } S^{\pm}_{mn}, \tag{8}$$

where

$$\tau = \frac{\rho\omega^2 dh^4}{-\omega^2 I - \mathrm{i}\omega\gamma + \kappa + C}. \tag{9}$$

The incident wave can be written in the form

$$\phi_{inc} = \mathrm{e}^{\mathrm{i}k(x\cos\theta + y\sin\theta)} N_0^{-1/2}\cosh k(z + h) = \mathrm{e}^{\mathrm{i}(\gamma_{00}x + \alpha_0 y)} N_0^{-1/2}\cosh k(z + h), \tag{10}$$

where $\gamma_{00} = k\cos\theta$, $\alpha_0 = k\sin\theta$ and $N_0 = (1 + \sinh 2kh/2kh)/2$. Since the paddles are arranged with periodicity $2d$ in the y direction, the fluid at $y + 2d$ only differs from that at y by $\mathrm{e}^{2\mathrm{i}\alpha_0 d}$, being a shift in phase of the incident wave. This implies

$$\phi(x, y + 2d, z) = \mathrm{e}^{2\mathrm{i}\alpha_0 d}\phi(x, y, z), \tag{11}$$

such that we only need to consider the solution in the strip $\{-\infty < x < \infty, |y| < d, -h < z < 0\}$ provided that

$$\phi(x, d, z) = \mathrm{e}^{2\mathrm{i}\alpha_0 d}\phi(x, -d, z) \quad \text{and} \quad \partial\phi(x, d, z)/\partial y = \mathrm{e}^{2\mathrm{i}\alpha_0 d}\partial\phi(x, -d, z)/\partial y. \tag{12}$$

The most general solution satisfying Eqs. (1)-(3) and (12) is

$$\phi = \sum_{p=0}^{\infty} \sum_{q=-\infty}^{\infty} \left(a_{pq} \mathrm{e}^{\mathrm{i}\gamma_{pq} x} + b_{pq} \mathrm{e}^{-\mathrm{i}\gamma_{pq} x} \right) \Psi_q(y) Z_p(z), \tag{13}$$

where $k_0 = -\mathrm{i}k$ ($k > 0$) and the positive real numbers k_p ($p > 1$) are the roots of the dispersion equation

$$\omega^2 = -g k_p \tan k_p h, \tag{14}$$

$$\alpha_q = \alpha_0 + q\pi/d, \tag{15}$$

and

$$\gamma_{pq} = \begin{cases} \sqrt{k^2 - \alpha_q^2}, & k \geq |\alpha_q|, p = 0, \\ \mathrm{i}\sqrt{\alpha_q^2 - k^2}, & k < |\alpha_q|, p = 0 \\ \mathrm{i}\sqrt{\alpha_q^2 + k_p^2}, & p \geq 0. \end{cases} \tag{16}$$

In Eq. (13) $\Psi_q(y)$ represent the eigenfunctions in the y direction, i.e.

$$\Psi_q(y) = \mathrm{e}^{\mathrm{i}\alpha_q y}, \tag{17}$$

satisfying the orthogonality relation

$$\frac{1}{2d} \int_{-d}^{d} \Psi_q(y) \Psi_p^*(y) \mathrm{d}y = \delta_{pq}, \tag{18}$$

in which δ_{pq} is the Kronecker delta symbol and the asterisk (*) denotes the complex conjugate. Also in Eq. (13), $Z_p(z)$ denote the eigenfunctions in the vertical direction, i.e.

$$Z_p = N_p^{-1/2} \cos k_p (z + h), \tag{19}$$

with

$$N_p = \frac{1}{2} \left(1 + \frac{\sin 2k_p h}{2k_p h} \right), \tag{20}$$

satisfying the orthogonality relation

$$\frac{1}{h} \int_{-h}^{0} Z_p(z) Z_q(z) \mathrm{d}z = \delta_{pq}, \tag{21}$$

Then we can write the general solution for $\phi(x, y, z)$ in two semi-infinite exterior regions as

$$\phi_0(x, y, z) = \phi_{inc} + \sum_{p=0}^{\infty} \sum_{q=-\infty}^{\infty} r_{pq} \mathrm{e}^{-\mathrm{i}\gamma_{pq} x} \Psi_q(y) Z_p(z), \quad \text{for } x < 0, \tag{22}$$

and

$$\phi_{M+1}(x, y, z) = \sum_{p=0}^{\infty} \sum_{q=-\infty}^{\infty} t_{pq} \mathrm{e}^{\mathrm{i}\gamma_{pq}(x - 2Mb)} \Psi_q(y) Z_p(z), \quad \text{for } x > 2Mb, \tag{23}$$

where r_{pq} and t_{pq} are the reflection and transmission coefficients to be determined.

From Eq. (16), we can see that γ_{pq} has $s^- + s^+ + 1$ real solutions, which represents the number of propogating modes, with

$$-s^- \leq q \leq s^+, \tag{24}$$

where

$$s^- = \left[\frac{kd}{\pi} (1 + \sin\theta) \right] \quad \text{and} \quad s^+ = \left[\frac{kd}{\pi} (1 - \sin\theta) \right], \tag{25}$$

in which $[x]$ denotes the integer part of x. Thus, in the exterior regions there exist at least one propagating mode ($q = 0$) in the x direction and higher order modes will be cut on at $kd = q\pi/(1 \pm \sin\theta)$ for $q = 1, 2, \cdots$.

Furthermore, we can also define the total reflected and transmitted energy ratios, R and T, as

$$R = \sum_{q=-s^-}^{s^+} \frac{\gamma_{0q}}{\gamma_{00}} |r_{0q}|^2 \quad \text{and} \quad T = \sum_{q=-s^-}^{s^+} \frac{\gamma_{0q}}{\gamma_{00}} |t_{0q}|^2. \tag{26}$$

Based on the conservation of energy, the dimensionless power that can be generated by M paddles in a single period $-d < y < d$, i.e. the efficiency of power capture, is

$$E_1(M) = 1 - R - T. \tag{27}$$

In addition, the total energy absorption of M paddles can also be determined by the sum of the power absorbed by each paddle, i.e.

$$E_2(M) = \frac{1}{E_{inc}} \sum_{m=1}^{M} E^{(m)} \tag{28}$$

which is an alternative expression for the efficiency of power capture, where $E_{inc} = \rho\omega dkh\cos\theta$ represents the incident wave power contained in the width $2d$ and the power generated by the mth paddle $E^{(m)}$ can be obtained by integrating the time-average product of pressure and velocity over the corresponding paddle surface

$$E^{(m)} = \frac{\rho\omega}{2} \mathrm{Im} \int_{-h}^{0} \int_{-c}^{c} \Delta\phi_{m0}(y,z) \frac{\partial\phi^*((2m-1)b, y, z)}{\partial x} \mathrm{d}y\mathrm{d}z. \tag{29}$$

By comparing the results of E_1 and E_2, we will be able to check the accuracy of the present semi-analytical model.

Next, we will show how to determine the general solution for $\phi(x, y)$ in the paddle array in order to obtain the reflection and transmission coefficients r_{pq} and t_{pq} in Eqs. (22) and (23).

3. Infinite paddle array

To determine the solution in the interior region $\{0 < x < 2Mb, y < |d|, -h < z < 0\}$, we follow the work of [29, 30] and first consider a homogeneous problem where the distribution of the paddle is extended to infinity in the x direction with period $2b$ (see Fig. 2). This allows us to use the Floquet-Bloch theory to consider a single fundamental cell in the infinite array and determine the corresponding eigensolutions. The single cell is defined by $D = \{0 < x < 2b, |y| < d, -h < z < 0\}$ with the outer boundary S.

The eigensolution $\psi(x, y, z)$, in addition to Eqs. (1)-(3), (8), (12), also satisfies the following Floquet-Bloch periodicity conditions

$$\left.\begin{aligned} \psi(2b, y, z) &= \mathrm{e}^{2\mathrm{i}\beta b}\psi(0, y, z) \\ \psi_x(2b, y, z) &= \mathrm{e}^{2\mathrm{i}\beta b}\psi_x(0, y, z) \end{aligned}\right\} \quad \text{for } |y| < d \text{ and } -h < z < 0, \tag{30}$$

where $\beta \in \mathbb{C}$ is the eigenvalue (or Floquet-Bloch wavenumber) to be determined. It is clear that if β is the solution to the above problem, so is $-\beta$ since we can replace x with $2b - x$.

3.1. Solution for $\psi(x, y, z)$

In view of Eq. (13), the general solution for $\psi(x, y, z)$ satisfying Eqs. (1)-(3) can be written as

$$\psi(x, y, z) = \begin{cases} \displaystyle\sum_{p=0}^{\infty} \sum_{q=-\infty}^{\infty} \left(a_{pq}\mathrm{e}^{\mathrm{i}\gamma_{pq}x} + b_{pq}\mathrm{e}^{-\mathrm{i}\gamma_{pq}(x-b)}\right)\Psi_q(y)Z_p(z), & 0 < x < b, \\ \displaystyle\sum_{p=0}^{\infty} \sum_{q=-\infty}^{\infty} \left(c_{pq}\mathrm{e}^{\mathrm{i}\gamma_{pq}(x-b)} + d_{pq}\mathrm{e}^{-\mathrm{i}\gamma_{pq}(x-2b)}\right)\Psi_q(y)Z_p(z), & b < x < 2b. \end{cases} \tag{31}$$

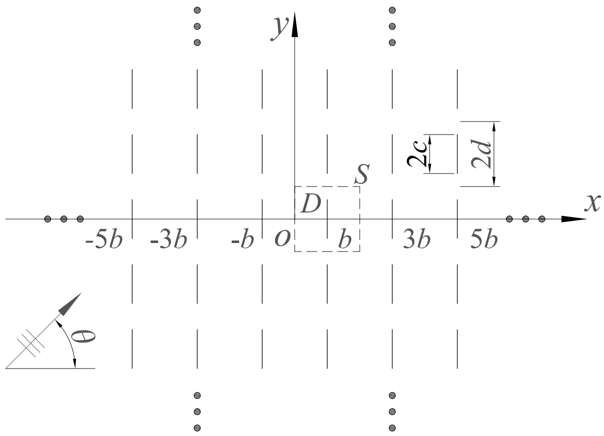

Figure 2: Infinite periodic paddle array.

Substituting Eq. (31) into Eq. (30) results in that

$$c_{pq} = \mathrm{e}^{2\mathrm{i}\beta b}\mathrm{e}^{-\mathrm{i}\gamma_{pq}b}a_{pq} \quad \text{and} \quad d_{pq} = \mathrm{e}^{2\mathrm{i}\beta b}\mathrm{e}^{\mathrm{i}\gamma_{pq}b}b_{pq}. \tag{32}$$

Since $\partial\psi/\partial x$ is continuous across $x = b$ for all $|y| < d$ and $-h < z < 0$, we have

$$\mathrm{e}^{\mathrm{i}\gamma_{pq}b}a_{pq} - b_{pq} = c_{pq} - \mathrm{e}^{\mathrm{i}\gamma_{pq}b}d_{pq}. \tag{33}$$

We define

$$\Delta\psi(y,z) = \psi(b^+,y,z) - \psi(b^-,y,z) = \begin{cases} P(y,z), & |y| < c, \\ 0, & c < |y| < d, \end{cases} \tag{34}$$

where $P(y,z)$ is the difference of the eigensolution over two sides of the paddle. If $P(y,z)$ is expanded as

$$P(y,z) = \sum_{p=0}^{\infty} P_p(y)Z_p(z), \tag{35}$$

then we can get

$$a_{pq} = \frac{1}{4d(\mathrm{e}^{2\mathrm{i}\beta b}\mathrm{e}^{-\mathrm{i}\gamma_{pq}b} - \mathrm{e}^{\mathrm{i}\gamma_{pq}b})}\int_{-c}^{c}\Psi_q^*(y)P_p(y)\mathrm{d}y, \tag{36}$$

after substituting Eq. (31) into Eq. (34) and using orthogonality relations (18) and (21). Applying the combined kinematic and dynamic condition (8) and substituting for a_{pq} by Eq. (36) gives

$$\sum_{p=0}^{\infty}\sum_{q=-\infty}^{\infty}\frac{\gamma_{pq}\sin(2\gamma_{pq}b)}{\cos(2\beta b) - \cos(2\gamma_{pq}b)}\Psi_q(y)Z_p(z)\int_{-c}^{c}\Psi_q^*(y')P_p(y')\mathrm{d}y' = \frac{4\tau f(z)}{h^4}\int_{-h}^{0}\int_{-c}^{c}\sum_{p=0}^{\infty}P_p(y)Z_p(z)f(z)\mathrm{d}y\mathrm{d}z. \tag{37}$$

If we multiply $Z_p(z)$ on the both sides of Eq. (37) and integrate over $-h < z < 0$, it results in the following scalar homogeneous integral equation

$$\sum_{q=-\infty}^{\infty}\frac{\gamma_{pq}\sin(2\gamma_{pq}b)}{\cos(2\beta b) - \cos(2\gamma_{pq}b)}\Psi_q(y)\int_{-c}^{c}\Psi_q^*(y')P_p(y')\mathrm{d}y' = \frac{4\tau V_p}{h}\sum_{l=0}^{\infty}V_l\int_{-c}^{c}P_l(y)\mathrm{d}y, \tag{38}$$

where

$$V_p = \frac{1}{h^2}\int_{-h}^{0}Z_p(z)f(z)\mathrm{d}z. \tag{39}$$

3.2. Numerical approximation

In order to solve Eq. (38), we can expand $P_p(y)$ in a series of orthogonal polynomials with weighted coefficients. Since the velocity potential at the two edges of the paddle, $(b, \pm c, -h < z < 0)$, behaves as the square root of the distance to the edge, we choose (see [31])

$$P_p(y) = \sum_{j=0}^{\infty} w_{pj} p_j(y), \tag{40}$$

where

$$p_j(y) = \frac{\sqrt{c^2 - y^2}\, U_j(y/c)}{(j+1)\pi c^2}, \tag{41}$$

in which $U(\cdot)$ is a second-kind Chebyshev polynomial.

Substituting the approximation (40) into Eq. (38), multiplying through by $p_k(y)$ and integrating over $-c < y < c$ leads to the following linear system of equations for the expansion coefficients w_{pj}

$$(\mathbf{L}^{(1)} - \tau \mathbf{L}^{(2)})\mathbf{W} = 0, \tag{42}$$

where $\mathbf{W} = \left\{w_{00}, w_{01}, \cdots, w_{pj}, \cdots, w_{\mathcal{P}\mathcal{J}}\right\}^{\mathrm{T}}$ for $p = 0, 1, 2, \cdots, \mathcal{P}$ and $j = 0, 1, 2, \cdots, \mathcal{J}$, and $\mathbf{L}^{(i)} = \left\{L^{(i)}_{p(\mathcal{J}+1)+k+1, q(\mathcal{J}+1)+j+1}\right\}$ for $i = 1, 2$, $q = 0, 1, 2, \cdots, \mathcal{P}$ and $k = 0, 1, 2, \cdots, \mathcal{J}$, whose entries are given by

$$L^{(1)}_{p(\mathcal{J}+1)+k+1, p(\mathcal{J}+1)+j+1} = \sum_{q=-\infty}^{\infty} \frac{\gamma_{pq} b \sin(2\gamma_{pq} b)}{\cos(2\beta b) - \cos(2\gamma_{pq} b)} F_{qk} F^*_{qj} \quad \text{and} \quad L^{(2)}_{p(\mathcal{J}+1)+k+1, q(\mathcal{J}+1)+j+1} = \delta_{k0}\delta_{j0}\frac{b}{h} V_p V_q, \tag{43}$$

in which

$$F_{qk} = \int_{-c}^{c} \Psi_q(y) p_k(y) \mathrm{d}y = \mathrm{i}^k \frac{J_{k+1}(\alpha_q c)}{\alpha_q c}, \tag{44}$$

(see [32]) and $J_k(\cdot)$ is the kth order Bessel function of the first kind. The system of equations (42) has been truncated by the parameters $\mathcal{J}$ and $\mathcal{P}$, where $\mathcal{J}$ denotes the number of terms used to approximate the difference of the velocity potential over the two sides of the paddle and $\mathcal{P}$ represents the number of vertical modes used to simulate the oscillation in the cell.

The solution to the Floquet-Bloch wavenumber β is obtained by identifying the non-trivial solution to the system of equations (42). This requires

$$\det\left(\mathbf{L}^{(1)} - \tau \mathbf{L}^{(2)}\right) = 0. \tag{45}$$

Although the entries $L^{(1)}_{uv}$ in $\mathbf{L^{(1)}}$ satisfy $L^{(1)}_{uv} = (-1)^{u+v} L^{(1)}_{vu}$ and $\mathbf{L^{(2)}}$ is real symmetric, it is still difficult to locate β in the complex plane directly from Eq. (45) because τ is complex. So here we first find the solution when $\mathrm{Im}[\tau] = 0$, which is denoted as β_0.

If we denote $\mathrm{e}^{2\mathrm{i}\beta_0 b}$ as λ_0 for the moment, it can be seen that λ_0^{-1} is also the solution of the corresponding problem after using $2b - x$ to replace x. We can also see that if ψ_0 is the solution corresponding to λ_0, then ψ_0^* is the solution corresponding to λ_0^*. As a consequence, λ_0 will lie either on the real axis in reciprocal pairs or on the unit circle in complex conjugate pairs. Returning to β_0, this implies that the pair values of $\pm\beta_0$ are either real numbers representing the waves propagating in opposite directions or can be expressed as complex numbers $n\pi/2b \pm \mathrm{i}\tilde{\beta}_{0,n}$ (where $n \in \mathbb{Z}$ and $\tilde{\beta}_{0,n} \in \mathbb{R}$) representing the evanescent waves decaying in opposite directions. Since replacing β_0 by $\beta_0 + n\pi/b$ leaves the problem unchanged, we only need to find the real values of $\beta_0 \in [0, \pi/2b]$ and the complex values of $\beta_0 = n\pi/2b \pm \mathrm{i}\tilde{\beta}_{0,n}$ for $n = 0, 1$. Now whether β_0 is real or complex, the matrix $\mathbf{L}^{(1)} + \mathrm{Re}[\tau]\mathbf{L}^{(2)}$ is hermitian such that its determinate is always real. A standard root-finding method thus can be applied to find β_0.

Next, taking β_0 as the initial value and gradually including the imaginary part of τ, we can track the path of each β in the complex plane until τ reaches the required value. Newton's method is used in the process of iteration. However, we find that compared to the case of the bottom-fixed plate given in [30], which is equivalent to letting $\tau = 0$ and $\mathcal{P} = 0$ in Eq. (42), more pure imaginary values of β_0 appear, and these values are very close to each other at some frequencies (see Fig. 3(b)). Besides, we also find that there exist repeated values of β_0 for some cases. Therefore, significant numerical effort is used accurately determining all possible values of β_0.

Another numerical strategy that avoids this effort involves finding roots β_0 at a single low frequency and using and then tracking values of β as the frequency increases. However, this method also encounters difficulties in some special cases. As the frequency increases, some values of β will be close to the origin (see Fig. 4(c)) or $\pi/2b$ (see Fig. 4 (a)), which means that β will become a near stationary point for the function $f(\beta) = \det\left(\mathbf{L}^{(1)} + \tau\mathbf{L}^{(2)}\right)$, i.e. $\mathrm{d}f(\beta)/\mathrm{d}\beta \approx 0$. As a result, the value of β at the chosen low frequency will give a poor initial estimate which may result in the failure of Newton's iteration algorithm. Therefore, in the actual numerical calculation, the two methods outlined above will be employed in combination; if one method fails, the other will be used. Additionally, in order to guarantee high computational efficiency a self-adaptive method is adopted when making small increments in Im[τ] or frequency, which can be referred to the Appendix B in [33].

3.3. Results

In this section, we first perform a convergence test of the numerical scheme for determining the Floquet-Bloch wavenumber β by varying the parameters $\mathcal{P}$ and $\mathcal{J}$ in the system of equations (42). We consider a paddle of length $c/d = 0.5$ with the dimensionless damping rate $\overline{\gamma} = \gamma/\sqrt{gh}\rho dh^3 = 0.4$ and spring constant $\overline{\kappa} = \kappa/\rho g dh^3 = 0.4$ in a fundamental cell with the spacing $b/d = 0.5$ and water depth $h/d = 2.0$ subject to an incidence with $\theta = \pi/6$. Tabs. 1-3 list the first three non-dimensional Floquet-Bloch wavenumbers $\beta^{(k)}h$ for $k = 1, 2, 3$, respectively. We can see that for both $\mathcal{P}$ and $\mathcal{J}$ only a few terms are needed to determine the results with nearly five significant figures. Note that for higher frequencies or $\beta^{(k)}$ with larger k, more terms are generally required to obtain the results with the same accuracy.

	$kh = 1.0$	$kh = 3.0$	$kh = 5.0$
$\mathcal{P} = 2, \mathcal{J} = 4$	1.0537 + 0.022252i	3.1467 + 0.42999i	3.7662 + 0.11020i
$\mathcal{P} = 4, \mathcal{J} = 4$	1.0537 + 0.022255i	3.1464 + 0.42988i	3.7657 + 0.11034i
$\mathcal{P} = 6, \mathcal{J} = 4$	1.0537 + 0.022256i	3.1464 + 0.42986i	3.7657 + 0.11035i
$\mathcal{P} = 8, \mathcal{J} = 4$	1.0537 + 0.022256i	3.1464 + 0.42986i	3.7657 + 0.11035i
$\mathcal{P} = 4, \mathcal{J} = 2$	1.0537 + 0.022255i	3.1464 + 0.42988i	3.7654 + 0.11034i
$\mathcal{P} = 4, \mathcal{J} = 6$	1.0537 + 0.022255i	3.1464 + 0.42988i	3.7658 + 0.11034i

Table 1: The convergence of the first Floquet-Bloch wavenumber $\beta^{(1)}h$ against the truncation parameters $\mathcal{P}$ and $\mathcal{J}$ for the case of $c/d = 0.5$, $\overline{\gamma} = 0.4$, $\overline{\kappa} = 0.4$, $b/d = 0.5$, $h/d = 2.0$ and $\theta = \pi/6$.

	$kh = 1.0$	$kh = 3.0$	$kh = 5.0$
$\mathcal{P} = 2, \mathcal{J} = 4$	−0.0077218 + 3.3895i	−0.0018183 + 3.0886i	4.4697 + 1.6828i
$\mathcal{P} = 4, \mathcal{J} = 4$	−0.0077230 + 3.3895i	−0.0018187 + 3.0886i	4.4722 + 1.6789i
$\mathcal{P} = 6, \mathcal{J} = 4$	−0.0077231 + 3.3895i	−0.0018187 + 3.0886i	4.4725 + 1.6785i
$\mathcal{P} = 8, \mathcal{J} = 4$	−0.0077231 + 3.3895i	−0.0018187 + 3.0886i	4.4726 + 1.6784i
$\mathcal{P} = 4, \mathcal{J} = 2$	−0.0077230 + 3.3895i	−0.0018187 + 3.0886i	4.4723 + 1.6789i
$\mathcal{P} = 4, \mathcal{J} = 6$	−0.0077230 + 3.3895i	−0.0018187 + 3.0886i	4.4722 + 1.6789i

Table 2: The convergence of the second Floquet-Bloch wavenumber $\beta^{(2)}h$ against the truncation parameters $\mathcal{P}$ and $\mathcal{J}$ for the case of $c/d = 0.5$, $\overline{\gamma} = 0.4$, $\overline{\kappa} = 0.4$, $b/d = 0.5$, $h/d = 2.0$ and $\theta = \pi/6$.

Before showing the results of the Floquet-Bloch wavenumber β, we first present the variation of the initial value of the iteration β_0 for the same case given in above. In Fig. 3(a), the blue line is the real value of β_0 and the red dashed line is the imaginary part of the complex values of $\beta_0 = \pi/2b + \mathrm{i}\tilde{\beta}_{0,1}$. Fig. 3(b) gives the imaginary part of the first six pure imaginary values of β_0. As described in [30], as the frequency increases, the value of β_0 on the imaginary axis will move along the negative direction until it reaches at the origin, and then a new real value of β_0 or propagating mode will cut on. The corresponding frequency is the cut-off frequency $kd = q\pi/(1 \pm \sin\theta)$ for $q = 1, 2, \cdots$, which is consistent with Eq. (25), since the eigenfunction $\psi(x, y)$ also satisfies the periodicity conditions (12). For the real

	$kh = 1.0$	$kh = 3.0$	$kh = 5.0$
$\mathcal{P} = 2, \mathcal{J} = 4$	$-0.031489 + 6.6251\mathrm{i}$	$-0.50521 + 4.4833\mathrm{i}$	$-0.010413 + 3.5449\mathrm{i}$
$\mathcal{P} = 4, \mathcal{J} = 4$	$-0.031493 + 6.6251\mathrm{i}$	$-0.50511 + 4.4830\mathrm{i}$	$-0.010383 + 3.5449\mathrm{i}$
$\mathcal{P} = 6, \mathcal{J} = 4$	$-0.031494 + 6.6251\mathrm{i}$	$-0.50510 + 4.4830\mathrm{i}$	$-0.010380 + 3.5449\mathrm{i}$
$\mathcal{P} = 8, \mathcal{J} = 4$	$-0.031494 + 6.6251\mathrm{i}$	$-0.50509 + 4.4830\mathrm{i}$	$-0.010379 + 3.5449\mathrm{i}$
$\mathcal{P} = 4, \mathcal{J} = 2$	$-0.031366 + 6.6227\mathrm{i}$	$-0.50479 + 4.4826\mathrm{i}$	$-0.010383 + 3.5449\mathrm{i}$
$\mathcal{P} = 4, \mathcal{J} = 6$	$-0.031493 + 6.6251\mathrm{i}$	$-0.50511 + 4.4830\mathrm{i}$	$-0.010383 + 3.5449\mathrm{i}$

Table 3: The convergence of the third Floquet-Bloch wavenumber $\beta^{(3)}h$ against the truncation parameters $\mathcal{P}$ and $\mathcal{J}$ for the case of $c/d = 0.5$, $\overline{\gamma} = 0.4$, $\overline{\kappa} = 0.4$, $b/d = 0.5$, $h/d = 2.0$ and $\theta = \pi/6$.

value of β_0, it will increase on the real axis until it is equal to $\pi/2b$, where the transverse standing mode will occur in the cell (see [30]) and the corresponding frequency is defined as the critical frequency (illustrated by the vertical dashed line in Fig. 3(a)). When the frequency exceeds the critical frequency, the values of β_0 will move off the real axis and follow the semi-infinite line $\beta_0 = \pi/2b + \mathrm{i}\tilde{\beta}_{0,1}$ where $\tilde{\beta}_{0,1} > 0$. Unlike the case of the bottom-fixed paddle (i.e. $\tau = 0$) (see [30]), the complex value of $\beta_0 = \pi/2b + \mathrm{i}\tilde{\beta}_{0,1}$ does not only exist above the first critical frequency and we have another complex value of β_0 for all frequencies. This value should be taken into account in some cases when considering the scattering problem.

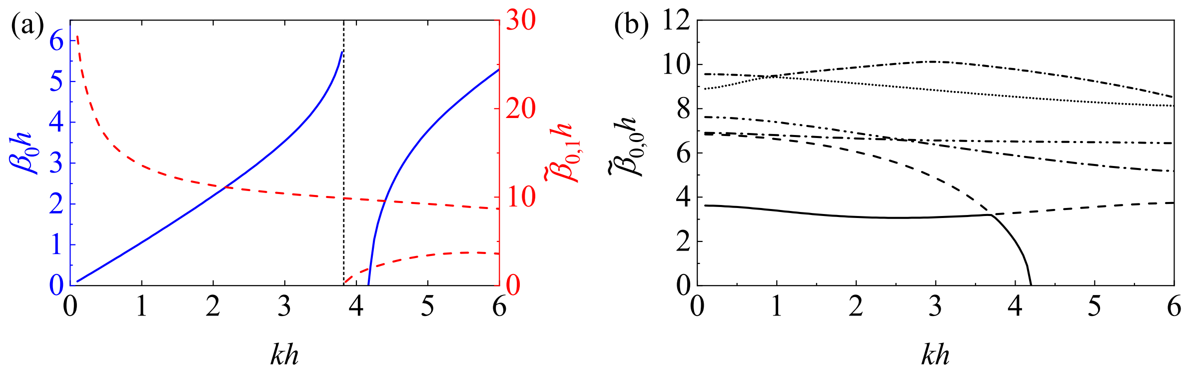

Figure 3: The variation of the initial value β_0 against the non-dimensional wavenumber kh for the case of $c/d = 0.5$, $\overline{\gamma} = 0.4$, $\overline{\kappa} = 0.4$, $b/d = 0.5$, $h/d = 2.0$ and $\theta = \pi/6$: (a) the real value (blue line) and the imaginary part of the complex value of $\beta_0 = \pi/2b + \mathrm{i}\tilde{\beta}_{0,1}$ (red dashed line); (b) the imaginary part of the first six pure imaginary values of $\beta_0 = \mathrm{i}\tilde{\beta}_{0,0}$.

Next, in Fig. 4 we give the variation of the first three non-dimensional Floquet-Bloch wavenumbers $\beta^{(k)}h$ against the non-dimensional wavenumber kh at different angles of incidence. Again, the same paddle and fundamental cell as above are considered. It should be noted that in principle we require $\mathrm{Im}[\beta^{(k+1)}] > \mathrm{Im}[\beta^{(k)}]$ if following the labelling rule given in the last section, but for clarity here we have exchanged the results between $\beta^{(1)}$, $\beta^{(2)}$ and $\beta^{(3)}$ at high frequencies so that we can obtain the smooth curve for each $\beta^{(k)}$. Additionally, Fig. 4 also includes the results of the initial values $\beta_0^{(k)}$. We can see that $\beta^{(k)}$ moves off the real or imaginary axis or the semi-infinite line $\pi/2b + \mathrm{i}\tilde{\beta}_{0,1}$ but still follows a similar variation trend of $\beta_0^{(k)}$. For $\beta_0^{(1)}$, if it is equal to $\pi/2b$, a transverse standing wave will occur in the corresponding cell. But when the paddle is connected to the damper, it is not possible for $\beta^{(1)}$ to be equal to $\pi/2b$ and standing mode will no longer occur.

Fig. 5 shows the variation of the first non-dimensional Floquet-Bloch wavenumber $\beta^{(1)}h$ for the paddle array with different spacings. From the cases of $b/d = 0.75$ and 1.0, we can see that with the increase of frequency, the value of β_0 on the semi-infinite line $\pi/2b + \mathrm{i}\tilde{\beta}_{0,1}$ will return to the real axis, decrease to the origin and then move along the negative imaginary axis. Thus, after the real part of the Floquet-Bloch wavenumber β reaches its maximum, which is around $\pi/2b$, both its real and imaginary parts will decrease with the frequency. For the case of $b/d = 0.25$, since β_0 will coincide with a branch of another complex root at $kh \approx 4.5$, we no longer calculate the β_0 from this frequency.

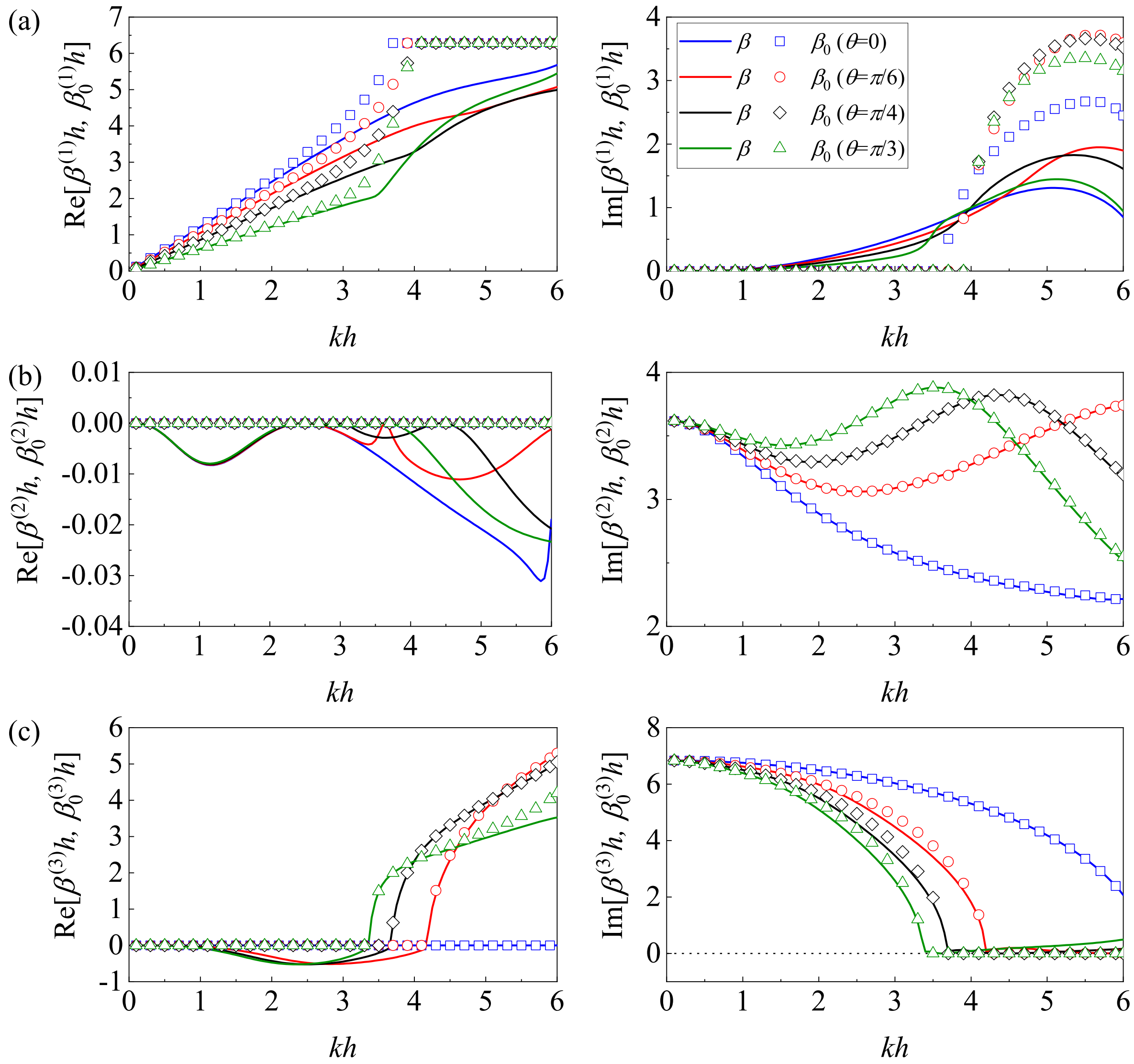

Figure 4: The variation of the non-dimensional Floquet-Bloch wavenumber $\beta^{(k)}h$ against the non-dimensional wavenumber kh for the case of $c/d = 0.5$, $\overline{\gamma} = 0.4$, $\overline{\kappa} = 0.4$, $b/d = 0.5$ and $h/d = 2.0$: (a) $k = 1$; (b) $k = 2$; (c) $k = 3$.

Alternatively, we use the β at the low frequency as the initial value to continue tracking the path of β.

The effects of the damping rate and spring constant on the first Floquet-Bloch wavenumber for the same cell given in Fig. 4 are illustrated in Fig. 6. We can see that at low frequencies the waves decay more rapidly through the paddle array with a smaller damping rate or spring constant, and the situation is reversed at high frequencies.

4. Wave scattering by multiple rows of paddle

Before we set about considering the scattering problem, we first introduce two sets of orthogonality relations. By means of Eq. (45), we can determine many eigenvalues of β and thus many corresponding eigenfunctions of ψ. For convenience, we first label the different eigenvalues as $\pm\beta^{(k)}$ ($k = 1, 2, \cdots$), which are ordered by their increasing imaginary parts, and label the corresponding eigenfunctions as $\psi^{(\pm k,+)}(x, y, z)$, where

$$\psi^{(-k,+)}(x, y, z) = \psi^{(+k,+)}(2b - x, y, z). \tag{46}$$

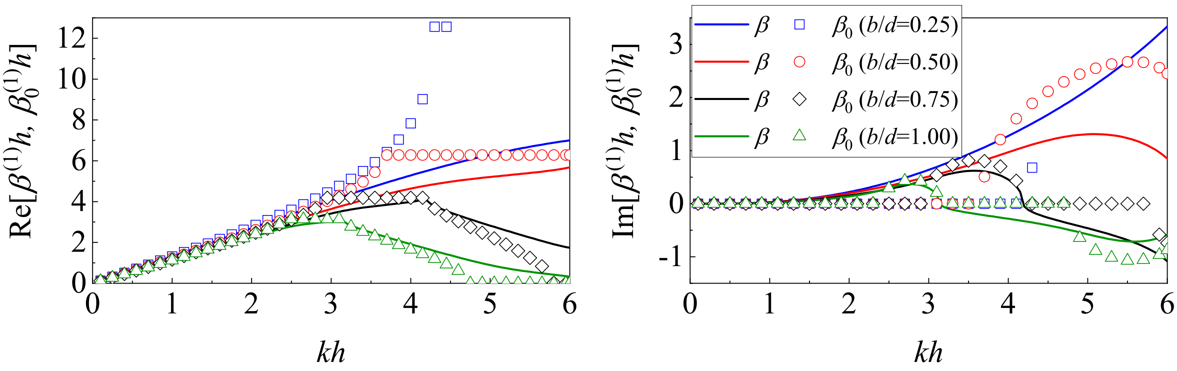

Figure 5: The variation of the first non-dimensional Floquet-Bloch wavenumber $\beta^{(1)}h$ against the non-dimensional wavenumber kh for the case of $c/d = 0.5$, $\overline{\gamma} = 0.4$, $\overline{\kappa} = 0.4$, $h/d = 2.0$ and $\theta = 0$.

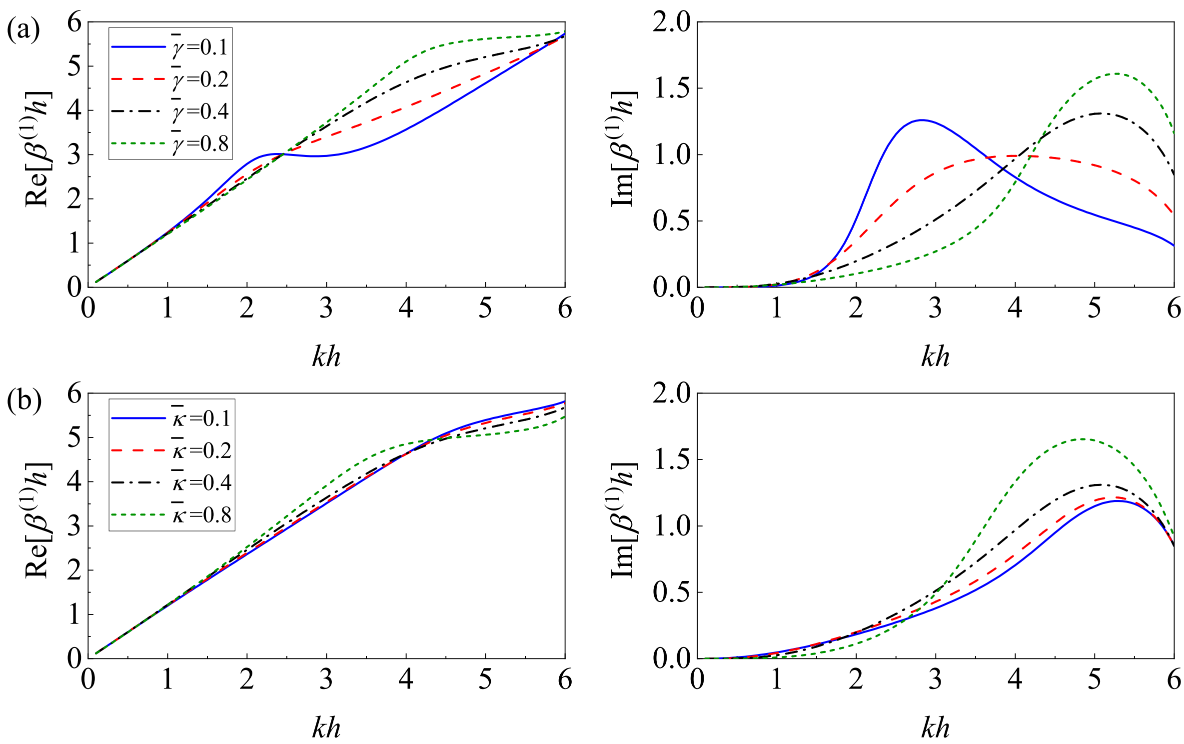

Figure 6: The variation of the first non-dimensional Floquet-Bloch wavenumber $\beta^{(1)}h$ against the non-dimensional wavenumber kh for the case of $c/d = 0.5$, $b/d = 0.5$, $h/d = 2.0$ and $\theta = 0$: (a) $\overline{\kappa} = 0.4$; (b) $\overline{\gamma} = 0.4$.

In addition, we also introduce another two eigenfunctions, $\psi^{(\pm k,-)}(x, y, z)$, given by

$$\psi^{(\pm k,-)}(x, y, z) = \psi^{(\pm k,+)}(x, -y, z). \tag{47}$$

such that $\psi^{(\pm k,-)}(x, y, z)$ satisfy the governing equation (1) and boundary conditions (2), (3), (8), (12) and (30) but with α_0 replaced with $-\alpha_0$. From Eqs. (46) and (47), we can see that $\psi^{(\pm k,+)}$ are the eigenmodes corresponding to the angles θ and $\pi - \theta$ and $\psi^{(\pm k,-)}$ corresponding to the angles $-\theta$ and $\pi + \theta$.

After some derivation (see Appendix A for the detailed derivation), we can find the following orthogonality relations

$$\int_{-h}^{0}\int_{-d}^{d}\left[\psi^{(+k,+)}\psi_x^{(+j,-)}-\psi^{(+j,-)}\psi_x^{(+k,+)}\right]_{x=0}\mathrm{d}y\mathrm{d}z=0, \tag{48a}$$

$$\int_{-h}^{0}\int_{-d}^{d}\left[\psi^{(+k,+)}\psi_x^{(-j,-)}-\psi^{(-j,-)}\psi_x^{(+k,+)}\right]_{x=0}\mathrm{d}y\mathrm{d}z=E^{(+k)}\delta_{kj}, \tag{48b}$$

and

$$\int_{-h}^{0}\int_{-d}^{d}\left[\psi^{(-k,+)}\psi_x^{(+j,-)}-\psi^{(+j,-)}\psi_x^{(-k,+)}\right]_{x=0}\mathrm{d}y\mathrm{d}z=E^{(-k)}\delta_{kj}, \tag{49a}$$

$$\int_{-h}^{0}\int_{-d}^{d}\left[\psi^{(-k,+)}\psi_x^{(-j,-)}-\psi^{(-j,-)}\psi_x^{(-k,+)}\right]_{x=0}\mathrm{d}y\mathrm{d}z=0. \tag{49b}$$

where $E^{(+k)}$ is the scaling factor.

Now, we return to considering the wave reflection and transmission of M rows of paddles (see Fig. 1), which is a finite section of the assumed infinite array considered above. The general solution of the velocity potential in $2(m-1)b < x < 2mb$ can now be written as a combination of the eigenfunctions $\psi^{(\pm k,+)}(x,y,z)$ of the above homogeneous problem, i.e.

$$\phi_m(x,y,z)=\sum_{k=1}^{\infty}\left[A_m^{(k)}\psi^{(+k,+)}(x-2(m-1)b,y,z)+\mathrm{e}^{2\mathrm{i}(M-1)\beta^{(k)}b}B_m^{(k)}\psi^{(-k,+)}(x-2(m-1)b,y,z)\right], \tag{50}$$

for $m=1,2,\cdots,M$, where $A_m^{(k)}$ and $B_m^{(k)}$ are undetermined coefficients. We first consider the following integrals, and it can be found that after substituting Eq. (50) into the integrals and using the orthogonality relations (48) and (49), the coefficients $A_m^{(k)}$ and $B_m^{(k)}$ can be separated out from the solution (50) and expressed explicitly, i.e.

$$\int_{-h}^{0}\int_{-d}^{d}\left[\phi_m(2mb,y,z)\frac{\partial\psi^{(-j,-)}}{\partial x}(0,y,z)-\psi^{(-j,-)}(0,y,z)\frac{\partial\phi_m}{\partial x}(2mb,y,z)\right]\mathrm{d}y\mathrm{d}z=\mathrm{e}^{2\mathrm{i}\beta^{(j)}b}E^{(+j)}A_m^{(j)}, \tag{51a}$$

$$\int_{-h}^{0}\int_{-d}^{d}\left[\phi_m(2mb,y,z)\frac{\partial\psi^{(+j,-)}}{\partial x}(0,y,z)-\psi^{(+j,-)}(0,y,z)\frac{\partial\phi_m}{\partial x}(2mb,y,z)\right]\mathrm{d}y\mathrm{d}z=\mathrm{e}^{2\mathrm{i}(M-2)\beta^{(k)}b}E^{(-j)}B_m^{(j)}, \tag{51b}$$

If a similar procedure is applied to ϕ_{m+1} and $\psi^{(\pm j,-)}$, we can obtain

$$\int_{-h}^{0}\int_{-d}^{d}\left[\phi_{m+1}(2mb,y,z)\frac{\partial\psi^{(-j,-)}}{\partial x}(0,y,z)-\psi^{(-j,-)}(0,y,z)\frac{\partial\phi_{m+1}}{\partial x}(2mb,y,z)\right]\mathrm{d}y\mathrm{d}z=E^{(+j)}A_{m+1}^{(j)}, \tag{52a}$$

$$\int_{-h}^{0}\int_{-d}^{d}\left[\phi_{m+1}(2mb,y,z)\frac{\partial\psi^{(+j,-)}}{\partial x}(0,y,z)-\psi^{(+j,-)}(0,y,z)\frac{\partial\phi_{m+1}}{\partial x}(2mb,y,z)\right]\mathrm{d}y\mathrm{d}z=\mathrm{e}^{2\mathrm{i}(M-1)\beta^{(k)}b}E^{(-j)}B_{m+1}^{(j)}. \tag{52b}$$

On the interface between two adjacent cells, continuity of pressure and velocity requires that

$$\phi_m(x,y,z)=\phi_{m+1}(x,y,z)\quad\text{and}\quad\partial\phi_m(x,y,z)/\partial x=\partial\phi_{m+1}(x,y,z)/\partial x,\quad\text{on } x=2mb,\ |y|<d,\ -h<z<0, \tag{53}$$

for $m=1,2,\cdots,M-1$. It should be noted that in this study we confine us to consider the case of $M\geq 2$ due to the matching conditions in Eq (53). According to Eqs. (51)-(53), we can confirm the relations between the coefficients

$$A_{m+1}^{(j)}=\mathrm{e}^{2\mathrm{i}\beta^{(j)}b}A_m^{(j)}\quad\text{and}\quad B_{m+1}^{(j)}=\mathrm{e}^{-2\mathrm{i}\beta^{(j)}b}B_m^{(j)}. \tag{54}$$

Eq. (54) confirms that the Floquet-Bloch eigenmodes do not couple with each other as waves propagate through the periodic array. Consequently, the general solution in the interior region can be expressed in terms of a single set of coefficients, $A_m^{(k)}$ and $B_m^{(k)}$, for any m. This implies that if we write

$$\phi_1(x,y,z)=\sum_{k=1}^{\infty}\left[A_1^{(k)}\psi^{(+k,+)}(x,y,z)+\mathrm{e}^{2\mathrm{i}(M-1)\beta^{(k)}b}B_1^{(k)}\psi^{(-k,+)}(x,y,z)\right], \tag{55}$$

as the general solution in $0 < x < 2b$, then the general solution in $2(M-1)b < x < 2Mb$ can be expressed as

$$\phi_M(x,y,z) = \sum_{k=1}^{\infty} \left[\mathrm{e}^{2\mathrm{i}(M-1)\beta^{(k)}b} A_1^{(k)} \psi^{(+k,+)}(x-2(M-1)b,y,z) + B_1^{(k)} \psi^{(-k,+)}(x-2(M-1)b,y,z) \right], \tag{56}$$

In order to determine the coefficients r_{pq} and t_{pq} in Eqs. (22) and (23), we still need to impose the remaining matching conditions on the common boundaries, which are

$$\phi_0(x,y,z) = \phi_1(x,y,z) \quad \text{and} \quad \partial\phi_0(x,y,z)/\partial x = \partial\phi_1(x,y,z)/\partial x, \quad \text{on } x=0,\, |y|<d,\, -h<z<0, \tag{57}$$

and

$$\phi_M(x,y,z) = \phi_{M+1}(x,y,z) \quad \text{and} \quad \partial\phi_M(x,y,z)/\partial x = \partial\phi_{M+1}(x,y,z)/\partial x, \quad \text{on } x=2Mb,\, |y|<d,\, -h<z<0. \tag{58}$$

Substituting Eqs. (22) and (55) into Eq. (57) gives

$$\delta_{p0}\delta_{q0} + r_{pq} = \sum_{k=1}^{\infty} \frac{2\cos(\gamma_{pq}b)\sin(\beta^{(k)}b)}{\sin[(\beta^{(k)}+\gamma_{pq})b]} a_{pq}^{(k)} \left(A_1^{(k)} + \mathrm{e}^{2\mathrm{i}\beta^{(k)}Mb} B_1^{(k)} \right), \tag{59a}$$

$$\delta_{p0}\delta_{q0} - r_{pq} = \sum_{k=1}^{\infty} \frac{2\sin(\gamma_{pq}b)\cos(\beta^{(k)}b)}{\sin[(\beta^{(k)}+\gamma_{pq})b]} a_{pq}^{(k)} \left(A_1^{(k)} - \mathrm{e}^{2\mathrm{i}\beta^{(k)}Mb} B_1^{(k)} \right), \tag{59b}$$

after using the orthogonality relations (18) and (21). After eliminating r_{pq} in Eq. (59), we have

$$\sum_{k=1}^{\infty} K_{pq,1}^{(k)} A_1^{(k)} + \sum_{k=0}^{\infty} K_{pq,2}^{(k)} B_1^{(k)} = \delta_{p0}\delta_{q0}, \tag{60}$$

where

$$K_{pq,1}^{(k)} = a_{pq}^{(k)} \quad \text{and} \quad K_{pq,2}^{(k)} = \frac{\tan(\beta^{(k)}b) - \tan(\gamma_{pq}b)}{\tan(\beta^{(k)}b) + \tan(\gamma_{pq}b)} \mathrm{e}^{2\mathrm{i}\beta^{(k)}Mb} a_{pq}^{(k)}. \tag{61}$$

Similarly, using Eqs. (23), (56) and (58) results in

$$t_{pq} = \sum_{k=1}^{\infty} \frac{2\cos(\gamma_{pq}b)\sin(\beta^{(k)}b)}{\sin[(\beta^{(k)}+\gamma_{pq})b]} a_{pq}^{(k)} \left(\mathrm{e}^{2\mathrm{i}M\beta^{(k)}b} A_1^{(k)} + B_1^{(k)} \right), \tag{62a}$$

$$t_{pq} = \sum_{k=1}^{\infty} \frac{2\sin(\gamma_{pq}b)\cos(\beta^{(k)}b)}{\sin[(\beta^{(k)}+\gamma_{pq})b]} a_{pq}^{(k)} \left(\mathrm{e}^{2\mathrm{i}M\beta^{(k)}b} A_1^{(k)} - B_1^{(k)} \right). \tag{62b}$$

Eliminating t_{pq} in Eq. (62) leads to

$$\sum_{k=1}^{\infty} K_{pq,2}^{(k)} A_1^{(k)} + \sum_{k=1}^{\infty} K_{pq,1}^{(k)} B_1^{(k)} = 0. \tag{63}$$

Note that if we write

$$A_s^{(k)} = A_1^{(k)} + B_1^{(k)} \quad \text{and} \quad A_a^{(k)} = A_1^{(k)} - B_1^{(k)}, \tag{64}$$

then the pair of equation systems above can be decoupled into

$$\sum_{k=1}^{\mathcal{K}} K_{pq,s/a}^{(k)} A_{s/a}^{(k)} = \delta_{p0}\delta_{q0}, \quad \text{for } p = 0,1,2,\cdots,\mathcal{P} \text{ and } q = -Q,-Q+1,\cdots,Q \tag{65}$$

where

$$K_{pq,s}^{(k)} = K_{pq,1}^{(k)} + K_{pq,2}^{(k)} \quad \text{and} \quad K_{pq,a}^{(k)} = K_{pq,1}^{(k)} - K_{pq,2}^{(k)}. \tag{66}$$

Eq. (64) is equivalent to decomposing the problem into a symmetric (s) and an antisymmetric (a) problem of the paddle array about its geometric plane of symmetry at $x = Mb$ from the outset. In order to solve Eq. (65) we set

$\mathcal{K} = (\mathcal{P}+1)\times(2\mathcal{Q}+1)$, where $\mathcal{P}+1$ and $2\mathcal{Q}+1$ represent, respectively, the eigenmodes in the z direction and y direction used to simulate the oscillation in the array. (It should be noted that the parameter $\mathcal{P}$ is identical to that given in Eq.(42).) Thus, we can see that the dimension of the systems of equations (65) depends on the number of eigenmodes considered and does not depend on the size of the array. Once the Floquet-Bloch wave number, $\beta^{(k)}$, and the corresponding eigenmode, $\psi^{(+k,+)}(x,y)$ or $a_{pq}^{(k)}$, for the single cell are determined, we can quickly obtain the results for any array size M.

4.1. Results

In this section, we also first perform a convergence test for the numerical scheme for determining the reflection and transmission coefficients by varying the truncation parameters $\mathcal{P}$ and $\mathcal{Q}$. An array consisting of five rows of paddles with the gap $a/d = 0.5$, spacing $b/d = 0.5$, damping rate $\overline{\gamma} = 0.4$ and spring constant $\overline{\kappa} = 0.4$ in the water of depth $h/d = 2.0$ at the incident wave angle $\theta = \pi/6$ is considered. The results of the efficiency of power capture calculated based on Eqs. (27) and (28) are both included in Tab. 4, where the results of E_2 are given in brackets. Comparison between E_1 and E_2 shows a high degree of accuracy of the present numerical method, and $\mathcal{P} = 4$ and $\mathcal{Q} = 4$ are generally sufficient to produce the results with an accuracy of about four significant figures.

	$kh = 1.0$	$kh = 3.0$	$kh = 5.0$
$\mathcal{P} = 2, \mathcal{Q} = 4$	0.10640 (0.10640)	0.84184 (0.84184)	0.58363 (0.58363)
$\mathcal{P} = 4, \mathcal{Q} = 4$	0.10642 (0.10642)	0.84181 (0.84180)	0.58439 (0.58439)
$\mathcal{P} = 6, \mathcal{Q} = 4$	0.10642 (0.10642)	0.84180 (0.84179)	0.58439 (0.58439)
$\mathcal{P} = 4, \mathcal{Q} = 2$	0.10642 (0.10642)	0.84180 (0.84184)	0.58429 (0.58441)
$\mathcal{P} = 4, \mathcal{Q} = 6$	0.10642 (0.10642)	0.84181 (0.84181)	0.58439 (0.58439)

Table 4: The convergence of the efficiency of power capture E_1 (E_2) against the truncation parameters $\mathcal{P}$ and $\mathcal{Q}$ for the case of $a/d = 0.5$, $b/d = 0.5$, $\overline{\gamma} = 0.4$, $\overline{\kappa} = 0.4$, $h/d = 2.0$, $\theta = \pi/6$ and $M = 5$.

We further validate our numerical model by comparing with results based on the wide-spacing approximation (WSA) proposed by [26] in which evanescent modes are neglected as waves propagate through the array and the method is valid only for the case of the normal incidence. From Fig. 7, it can be seen that the results of the two methods are in good agreement for spacings $b/d \gtrsim 0.5$. For the case of narrow spacing, the results of WSA remain remarkably good although tend to overestimate energy absorption.

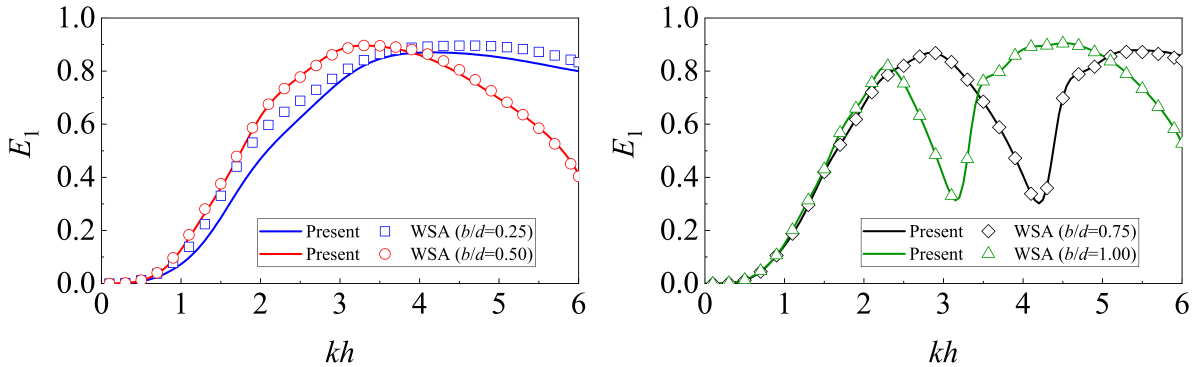

Figure 7: Comparison of the efficiency of power capture, E_1, between the present model and wide-spacing approximation (WSA) proposed by [26] for the case of $a/d = 0.5$, $\overline{\gamma} = 0.4$, $\overline{\kappa} = 0.4$, $h/d = 2.0$, $\theta = 0$ and $M = 5$.

Furthermore, [26] did not produce results that directly show the effect of plate array mechanics on efficiency and we continue with some results which illustrate different effects within the proposed wave energy device. The wave energy absorbed at different incident wave angles is shown in Fig. 8. At low frequencies, the array performs best at normal incidence and a small change in the angle of incidence will have little effect on the energy absorption efficiency.

At some high frequencies, the array subjected to a plane wave with a larger incident wave angle may generate more energy.

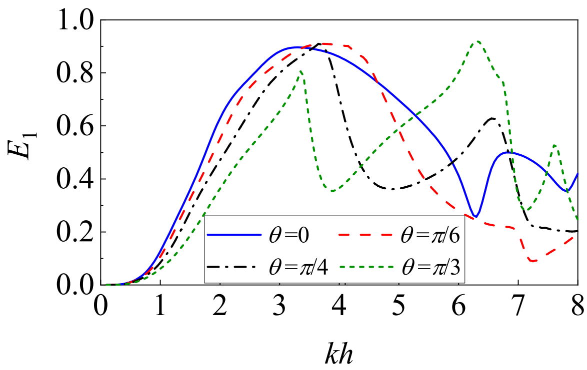

Figure 8: The variation of the efficiency of power capture, E_1, against the non-dimensional wavenumber kh for the case of $a/d = 0.5$, $b/d = 0.5$, $\overline{\gamma} = 0.4$, $\overline{\kappa} = 0.4$, $h/d = 2.0$ and $M = 5$.

Correspondingly, the horizontal displacements and phases of the hinged paddles at the mean surface of the fluid under a regular incident wave of amplitude A are shown in Fig. 9. When a long wave propagates through the array, the oscillation amplitude of the paddle on the downstream is relatively large due to the interference effect. As frequency increases, the sheltering effect leads to a relatively small pitch angle of the downstream paddle. For the different incident wave angles, the normal incidence results not only in a high efficiency of energy absorption (see Fig. 8) but also in large oscillations of the paddles. Moreover, a large number of studies (e.g. [9, 20, 34, 35, 36]) have reported the spiky behaviour of hydrodynamic forces and coefficients occurring at cut-off frequencies, i.e. $kd = q\pi(1 \pm \sin\theta)$ $(q = 1, 2, \cdots)$, for a periodic array. In the present study, similar spikes can also be observed in Fig. 9(b)(c)(d), although the spring and damping considered in the configuration smooth the curves. However, the spikes are not obvious for the energy absorption when the incident wave angle is $\pi/6$ or $\pi/4$ (see Fig. 8). This can be attributed to the result of the superposition of the curve of each paddle.

The effect of the damping rate and spring constant is shown in Figs. 10 and 11. Fig. 10 shows the effect on the motion of the paddle. When the damping and spring are "switched off", the paddle will resonate at the low frequency. As the damping rate and spring constant increase, the motion of the paddle is quickly suppressed. From Fig. 11, we can see that for the present case the optimal damping rate $\overline{\gamma}$ is between 0.1 and 0.2, and the array behaves with a high efficiency of wave absorption over a wide frequency. For the spring constant $\overline{\kappa}$, its variation from 0.1 to 0.4 has a limited effect on the wave energy absorption efficiency.

Finally, we change the number of rows to $M = 2$ and $M = 8$ so that a smaller and a larger array are considered. Fig. 12(a) shows the variation of the efficiency against the non-dimensional wavenumber kh and each array has the same setting as that given in Fig. 7. Besides, the results for the case of a single row array ($M = 1$) are also included in Fig. 12(a), which is based on the method of Section 3 without including periodic conditions (30). We can see that in the considered frequency range increasing the number of paddles can improve the total power absorption efficiency. In order to evaluate the energy generation performance of the entire array and each row of the array respectively, we follow [12] to define two following factors

$$\bar{q} = E_1(M)/ME_1(M = 1), \tag{67}$$

and

$$q^{(m)} = E^{(m)}/E_{inc}E_1(M = 1) \tag{68}$$

such that $M\bar{q} = \sum_{m=1}^{M} q^{(m)}$. $\bar{q} > 1$ implies that the multi-row paddle array produces a global constructive effect from the interference compared to the isolated single-row paddle array, and $q^{(m)} > 1$ means that the mth row paddle array benefits from the interaction between multiple rows of paddles. It is not surprising that in most cases $\bar{q} < 1$. This is because as the waves propagate through the array, the energy is gradually consumed by the paddle in front of the array. The paddle on the downstream contributes less to power generation compared with the case of an isolated single-row

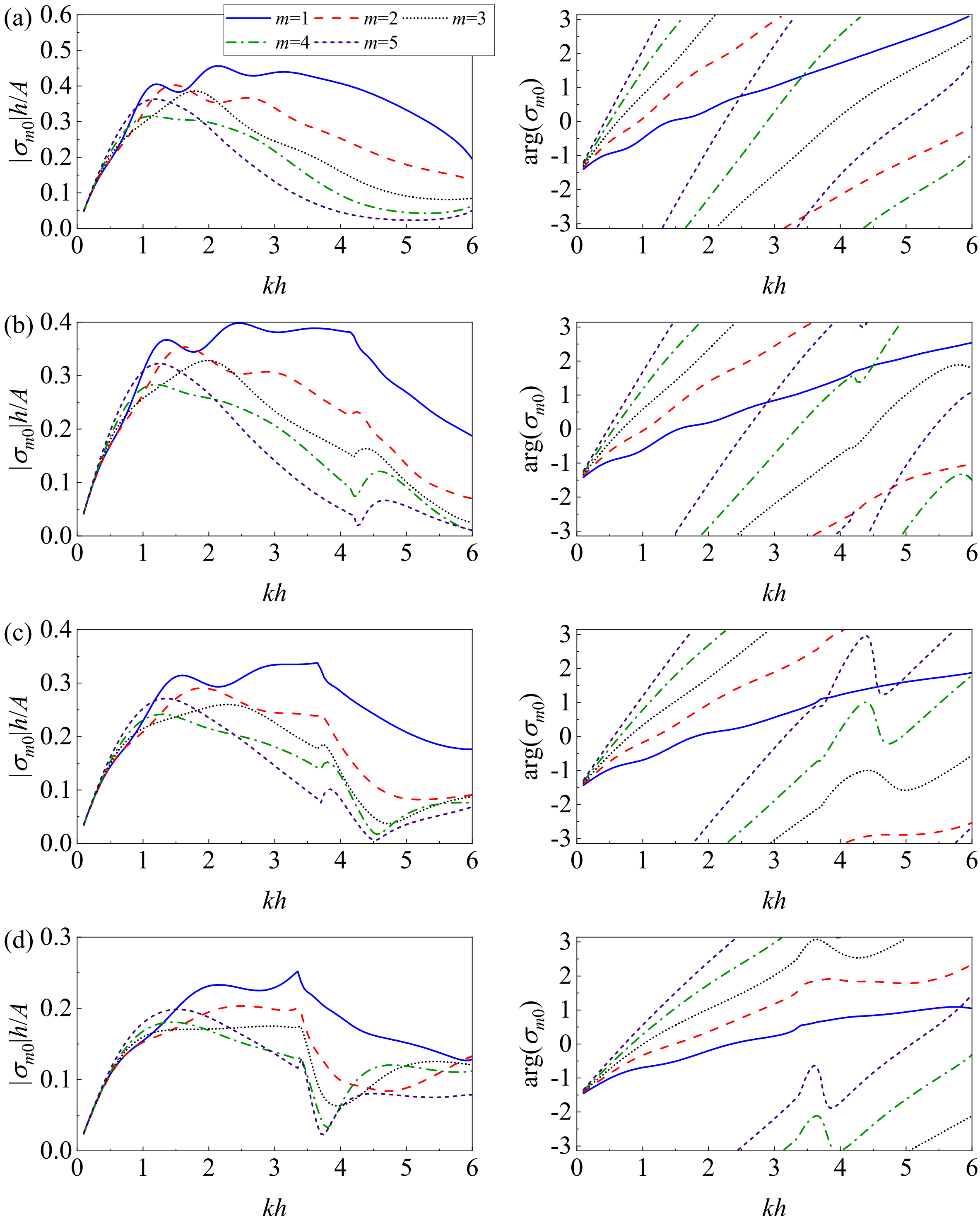

Figure 9: The horizontal displacements and phases of the hinged paddles at the mean surface of the fluid, σ_{m0}, against the non-dimensional wavenumber kh for the case of $a/d = 0.5$, $b/d = 0.5$, $\overline{\gamma} = 0.4$, $\overline{\kappa} = 0.4$, $h/d = 2.0$ and $M = 5$: (a) $\theta = 0$; (b) $\theta = \pi/6$; (c) $\theta = \pi/4$; (d) $\theta = \pi/3$.

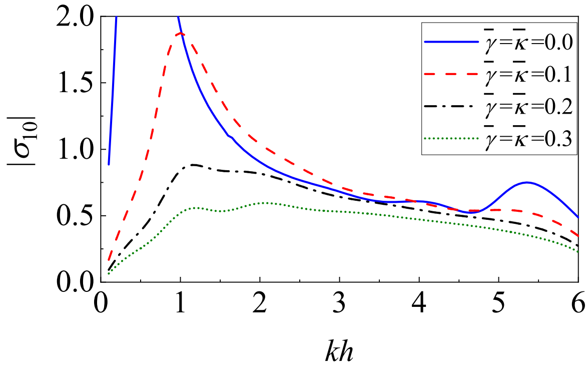

Figure 10: The horizontal displacement of the first hinged paddles ($m = 1$) at the mean surface of the fluid, σ_{01} against the non-dimensional wavenumber kh for the case of $a/d = 0.5$, $b/d = 0.5$, $h/d = 2.0$, $\theta = 0$ and $M = 5$.

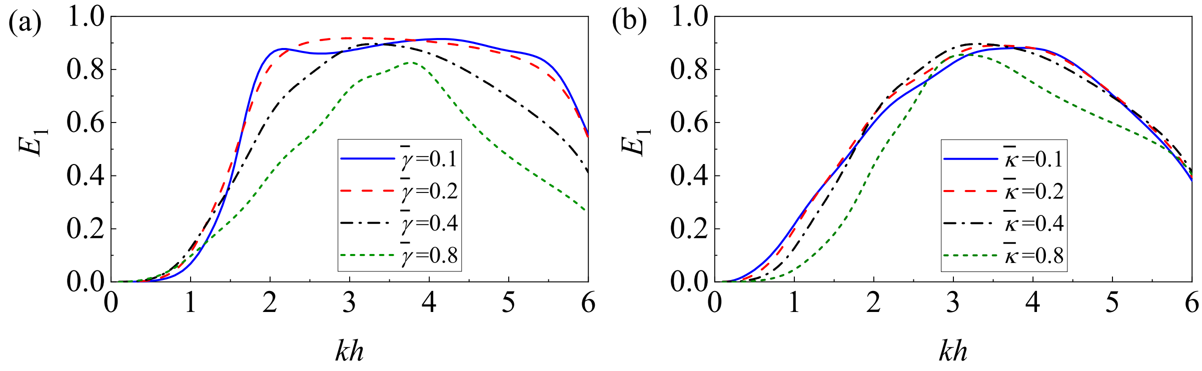

Figure 11: The variation of the efficiency of power capture, E_1, against the non-dimensional wavenumber kh for the case of $a/d = 0.5$, $b/d = 0.5$, $h/d = 2.0$, $\theta = 0$ and $M = 5$: (a) $\bar{\kappa} = 0.4$; (b) $\bar{\gamma} = 0.4$.

paddle array, resulting in a lower averaged value of $\bar{q}$. For $q^{(m)}$, we can see that only the first-row paddle array could exhibit an enhanced performance, which can be attributed to the reflection of the downstream paddles. These results are consistent with those in [12] who considered two parallel wave farms, each consisting of 13 in-line oscillating wave surge converters.

5. Conclusion

In this study we have considered a periodic array consisting of a finite number of rows of vertical thin paddles hinged at sea bottom, each row including an infinite number of paddles arranged in a line. Each paddle is connected to its own damper and spring, allowing wave energy to be absorbed from water waves from the pitching motion.

The mathematical approach to the solution of this problem has involved first determining Floquet-Bloch eigensolutions to a homogeneous problem which is represented by the corresponding infinite array problem. Since a linear damping mechanism is considered, Floquet-Bloch eigenvalues are found in the complex plane and locating these eigenvalues is the most numerically challenging part of the method. Two approaches are used in combination to track solutions from low frequencies and from zero damping where eigenvalues are easier to find. The eigenfunctions satisfy an orthogonality relation which works for waves propagating in geometrically opposing directions and which holds regardless of the geometry of the structure. Once the eigenvalues and eigenfunctions are determined, the general solution of the velocity potential can be written as a superposition of these eigenfunctions. After applying the matching conditions and orthogonality relations, we can obtain simple low-order systems of equations that are independent of the number of rows in the array.

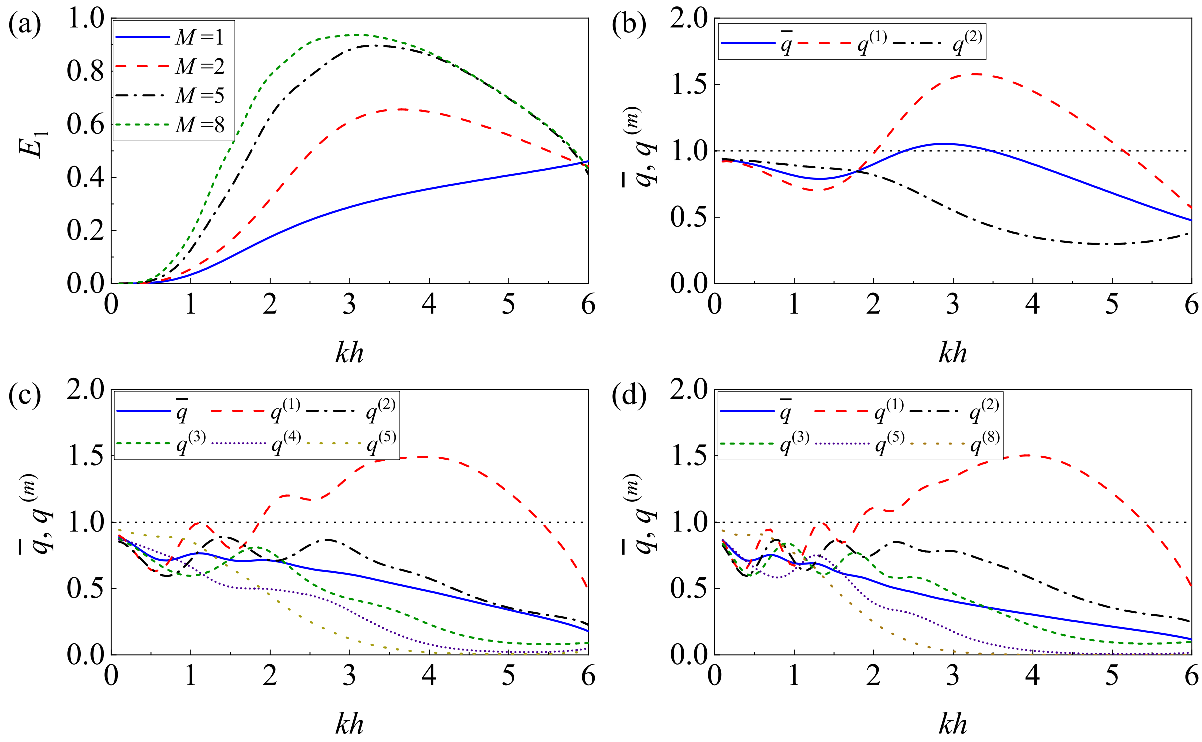

Figure 12: (a) The variation of the efficiency of power capture, E_1, against the non-dimensional wavenumber kh for the case of $a/d = 0.5$, $b/d = 0.5$, $\bar{\gamma} = 0.4$, $\bar{\kappa} = 0.4$, $h/d = 1.0$ and $\theta = 0$; The energy generated by the mth paddle for the array of (b) $M = 2$; (c) $M = 5$; (d) $M = 8$.

Our results for arbitrary incident wave angle and row-spacing have been compared with the approximation of [26] based on a wide-spacing assumption and normal wave incidence. Moreover, a parametric study has been carried out to investigate the power extraction efficiency. Multiple rows of pitching paddle devices show that a high broadband output across a wide range of frequencies is possible, particularly with low damping and larger numbers of rows. As the number of paddle rows increases, the efficiency of the whole array power generation improves, but only the first row can enjoy the beneficial effect and the gains from adding further rows diminish rapidly, resulting in a lower averaged energy absorption when compared to an isolated single row paddle array.

Acknowledgement

The work was supported by the EPSRC, grant number EP/V04740X/1.

Declaration of interests

The authors report no conflict of interest.

Appendix A. Orthogonality relations for the Floquet-Bloch eigenmodes of a single cell

In this Appendix, we present two sets of orthogonality relations which will be widely used in the scattering problem. Applying Green's second identity to $\psi^{(+k,+)}$ and $\psi^{(\pm j,-)}$, we first have

$$\iiint_D \left[\psi^{(+k,+)}\nabla^2\psi^{(\pm j,-)} - \psi^{(\pm j,-)}\nabla^2\psi^{(+k,+)}\right]\mathrm{d}v = \iint_{S_{00}^{\pm}+S} \left[\psi^{(+k,+)}\partial\psi^{(\pm j,-)}/\partial n - \psi^{(\pm j,-)}\partial\psi^{(+k,+)}/\partial n\right]\mathrm{d}s, \quad \text{(A.1)}$$

where ds is the elemental arclength of S and $S_{00}^{\pm}$ with outward normal derivative $\partial/\partial n$. With the employment of the condition (8), we can see that the integral on $S_{00}^{\pm}$ vanishes. Thus Eq. (A.1) becomes

$$\left[\mathrm{e}^{2\mathrm{i}(\beta^{(k)}\pm\beta^{(j)})b}-1\right]\int_{-h}^{0}\int_{-d}^{d}\left[\psi^{(+k,+)}\psi_x^{(\pm j,-)}-\psi^{(\pm j,-)}\psi_x^{(+k,+)}\right]_{x=0}\mathrm{d}y\mathrm{d}z=0, \tag{A.2}$$

after using Eqs. (30), (46) and (47). Since $\beta^{(k)}\in\mathbb{C}$, as long as $k\neq j$ the factor in front of the integral in (A.2) will not be zero. Thus, we have the orthogonality relation (48). Similarly, applying Green's second identity to $\psi^{(-k,+)}$ and $\psi^{(\pm j,-)}$ leads to another set of orthogonality relation (49). Using Eqs. (46) and (47), it can be found that $E^{(-k)}=-E^{(+k)}$. From Eqs. (48) and (49) we can see that two eigenmodes with opposite directions are orthogonal to each other. Note that the orthogonality relations (48) and (49) hold regardless of the geometry of the structure.

References

[1] S. Salter, Wave energy: Nostalgic ramblings, future hopes and heretical suggestions, J. Ocean Eng. and Marine Energy 2 (2016) 399–428.
[2] S. Salter, Wave power, Nature 249 (1974) 720–724.
[3] A. Babarit, A database of capture width ratio of wave energy converters, Renew. Energy 80 (2015) 610–628.
[4] C. C. Mei, M. A. Stiassnie, D. K. P. Yue, Theory and applications of ocean surface waves: Part 1: linear aspects, World Scientific, 2005.
[5] T. Whittaker, M. Folley, Nearshore oscillating wave surge converters and the development of the oyster, Phil. Trans. R. Soc. Lond A. 370 (2012) 345–364.
[6] E. Renzi, F. Dias, Hydrodynamics of the oscillating wave surge converter in the open ocean, Eur. J. Mech B. Fluids 41 (2013) 1–10.
[7] I. Noad, R. Porter, Optimisation of arrays of flap-type oscillating wave surge converters, Appl. Ocean Res. 50 (2015) 237–253.
[8] R. Gomes, M. Lopes, J. Henriques, L. Gato, A. Falcão, The dynamics and power extraction of bottom-hinged plate wave energy converters in regular and irregular waves, Ocean Eng. 96 (2015) 86–99.
[9] E. Renzi, F. Dias, Resonant behaviour of an oscillating wave energy converter in a channel, J. Fluid Mech. 701 (2012) 482–510.
[10] E. Renzi, F. Dias, Relations for a periodic array of flap-type wave energy converters, Appl. Ocean Res. 39 (2013) 31–39.
[11] P. Sammarco, S. Michele, M. d'Errico, Flap gate farm: From venice lagoon defense to resonating wave energy production. part 1: Natural modes, Appl. Ocean Res. 43 (2013) 206–213.
[12] D. Sarkar, E. Renzi, F. Dias, Wave farm modelling of oscillating wave surge converters, Proc. Roy. Soc. A 470 (2014) 20140118.
[13] D. Sarkar, E. Renzi, F. Dias, Effect of a straight coast on the hydrodynamics and performance of the oscillating wave surge converter, Ocean Eng. 105 (2015) 25–32.
[14] D. Sarkar, E. Contal, N. Vayatis, F. Dias, Prediction and optimization of wave energy converter arrays using a machine learning approach, Renew. Energy 97 (2016) 504–517.
[15] S. Michele, E. Renzi, P. Sammarco, Weakly nonlinear theory for a gate-type curved array in waves, J. Fluid Mech. 869 (2019) 238–263.
[16] C. Mei, Resonant reflection of surface water waves by periodic sandbars, J. Fluid Mech. 152 (1985) 315–335.
[17] R. Porter, D. Porter, Scattered and free waves over periodic beds, J. Fluid Mech. 483 (2003) 129–163.
[18] C. Linton, D. Evans, The interaction of waves with arrays of vertical circular cylinders, J. Fluid Mech. 215 (1990) 549–569.
[19] C. Mei, I. Chan, P.-F. Liu, Waves of intermediate length through an array of vertical cylinders, Environ. Fluid Mech. 14 (2014) 235–261.
[20] R. Porter, D. Evans, Wave scattering by periodic arrays of breakwaters, Wave motion 23 (1996) 95–120.
[21] R. Porter, Plate arrays as a perfectly-transmitting negative-refraction metamaterial, Wave Motion 100 (2021) 102673.
[22] J. Hu, C. Mei, C.-H. Chang, P. Liu, Effect of flexible coastal vegetation on waves in water of intermediate depth, Coastal Eng. 168 (2021) 103937.
[23] X. Garnaud, C. C. Mei, Wave-power extraction by a compact array of buoys, J. Fluid Mech. 635 (2009) 389–413.
[24] D. Ko, J. Sambles, Scattering matrix method for propagation of radiation in stratified media: attenuated total reflection studies of liquid crystals., J. Opt. Soc. Am. A 5 (1988) 1863–1866.
[25] C. M. Linton, P. McIver, Handbook of mathematical techniques for wave/structure interactions, 2001.
[26] A. Mérigaud, B. Thiria, R. Godoy-Diana, A wide-spacing approximation model for the reflection and transmission of water waves over an array of vertical obstacles, J. Fluid Mech. 923 (2021) A2.
[27] M. Göteman, Multiple cluster scattering with applications to wave energy park optimizations, Appl. Ocean Res. 125 (2022) 103256.
[28] C. Mei, I. Chan, P. Liu, Z. Huang, W. Zhang, Long waves through emergent coastal vegetation, J. Fluid Mech. 687 (2011) 461–491.
[29] J. Huang, R. Porter, Water wave propagation through arrays of closely-spaced surface-piercing vertical barriers, J. Fluid Mech. 960 (2023) A20.
[30] J. Huang, R. Porter, Scattering of water waves by multiple rows of vertical thin barriers, Wave motion (To be published) (2023).
[31] R. Porter, D. Evans, Complementary approximations to wave scattering by vertical barriers, J. Fluid Mech. 294 (1995) 155–180.
[32] H. Bateman, Tables of integral transforms, volume 1, McGraw-Hill Book Company, 1954.
[33] J. Huang, R. Porter, S. Zheng, A surface-piercing truncated cylindrical meta-structure operating as a wave energy converter, Phys. Fluids (2023).
[34] C. Linton, D. Evans, F. Smith, The radiation and scattering of surface waves by a vertical circular cylinder in a channel, Proc. Roy. Soc. A 338 (1992) 325–357.
[35] M. Fernyhough, D. Evans, Scattering by periodic array of rectangular blocks, J. Fluid Mech. 305 (1995) 263–279.
[36] J. Huang, B. Teng, The second-order interaction of monochromatic waves with three-dimensional bodies in a channel, Ocean Eng. 217 (2020) 107951.